Tet Repressor Induction without Mg^{2+} †

Oliver Scholz, Peter Schubert, Martin Kintrup, and Wolfgang Hillen*

Lehrstuhl für Mikrobiologie, Institut für Mikrobiologie, Biochemie und Genetik, Friedrich-Alexander Universität Erlangen-Nürnberg, Staudtstrasse 5, 91058 Erlangen, Germany

Received May 4, 2000; Revised Manuscript Received June 26, 2000

ABSTRACT: We have examined anhydrotetracycline (atc) binding to Tet repressor (TetR) in dependence of the Mg^{2+} concentration. Of all tc compounds tested so far, atc has the highest affinity for TetR, with a K_A of 9.8×10^{11} M^{-1} in the presence of Mg^{2+} and 6.5×10^7 M^{-1} without Mg^{2+}. Thus, it binds TetR with 500-fold higher affinity than tc under both conditions. The Mg^{2+}-free binding of atc to TetR leads to induction in vitro, demonstrating that the metal is not necessary to trigger the associated conformational change. To obtain more detailed information about Mg^{2+}-free induction, we constructed and prepared to homogeneity four single-alanine substitution mutants of TetR. Three of them affect residues involved in contacting Mg^{2+} (TetR H100A, E147A, and T103A), and one altered residue contacts tc TetR N82A. TetR H100A and E147A are induced by atc, with and without Mg^{2+}, showing 110-fold and 1000-fold decreased Mg^{2+}-dependent and unchanged Mg^{2+}-independent atc binding, respectively. Thus, the contacts of these residues to Mg^{2+} are not necessary for induction. TetR N82A is not inducible under any of the conditions employed and shows an about 4000-fold decreased atc binding constant. The Mg^{2+}-dependent affinity of TetR T103A for atc is only 400-fold reduced, but no induction with atc was observed. Thus, Thr103 must be essential for the conformational change associated with induction in the absence of Mg^{2+}.

Tetracycline (tc)[1] is an inhibitor of bacterial protein biosynthesis (*1*) and shows only little toxicity for eukaryotic cells. Tc is complexed with a divalent metal ion, presumably Mg^{2+} in vivo, to exert its biological function. The $[tc-Me]^+$ complex is also the inducer of Tet repressor (TetR), controlling expression of tc resistance in Gram-negative bacteria. The binding constant of the $[tc-Mg]^+$ complex and TetR is approximately 10^9 M^{-1}, dropping to about 10^5 M^{-1} in the absence of Mg^{2+} (*2*). The $[tc-Fe]^+$ complex is more stable than $[tc-Mg]^+$ and is an active inducer. Fe^{2+}-dependent oxidative cleavage of TetR using Fenton chemistry leads to a map of residues located close to the ion (*3*). Consequently, no induction has been observed in the absence of divalent cations in vitro (*3*). The results of the Fe^{2+} cleavage and Mg^{2+} binding studies suggest an important role of Me^{2+} for induction. The crystal structures of TetR in complex with $[tc-Mg]^+$ and *tet* operator provide snapshots for the starting point and endpoint of TetR induction (*4*−*6*). The crystallographic data also suggest that Mg^{2+} plays a crucial role in the mechanism of induction, since the initial structural changes of TetR occur at residues His100 and Thr103, which contact Mg^{2+} in the crystal structure of the TetR−$[tc-Mg]^+$ complex (*6*−*8*). Despite its chemical similarity to tc, anhydrotetracycline (atc, see Figure 1) exhibits a bactericidal effect on bacteria (*9*) and increased cytotoxicity for eukaryotic cells (*10*). Nevertheless, atc is a very efficient inducer of TetR. In this study we establish that atc can bind with considerable affinity to and induce TetR in vitro in the absence of Mg^{2+}. We demonstrate further, that substitution of residues His100 and Thr103 by Ala leads to TetR mutants which are not induced by $[tc-Mg]^+$ or tc. However, TetR H100A is fully inducible by atc without Mg^{2+} while TetR T103A is not. Thus, Thr103 seems to be a key residue for induction, regardless of the presence of a divalent metal ion. A Mg^{2+}-free inducer could be important for potential eukaryotic applications of TetR-based regulatory systems, because the passage of inducers across biological barriers such as some cell envelopes or the blood−brain barrier may be enhanced if they do not form charged complexes.

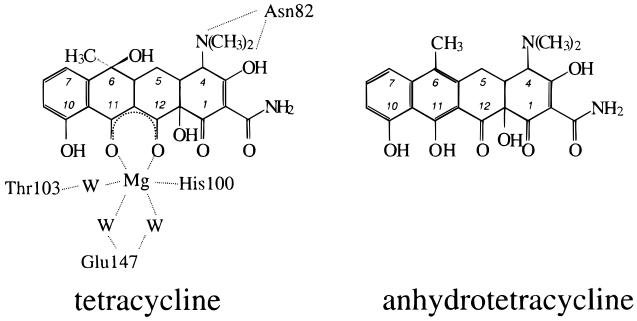

FIGURE 1: Chemical structures of tetracycline and anhydrotetracycline. Some contacting amino acids are shown for tetracycline. The three Mg^{2+}-coordinating water molecules are designated as "W".

EXPERIMENTAL PROCEDURES

Materials and General Methods. Atc was purchased from Acros (Geel, Belgium) and tc from Merck (Darmstadt,

† This work was supported by the Deutsche Forschungsgemeinschaft (DFG) through the SFB 473 and the Fonds der Chemischen Industrie (FCI).

* To whom correspondence should be addressed. Phone: +49 9131/85-28081, Fax: +49 9131/85-28082, Email: whillen@biologie.uni-erlangen.de.

[1] Abbreviations: tc, tetracycline; atc, anhydrotetracycline; TetR, Tet repressor.

10.1021/bi001018p CCC: $19.00
Published on Web 08/11/2000

Germany). All other chemicals are from Merck (Darmstadt, Germany) or Roth (Karlsruhe, Germany) or Sigma (München, Germany) at the highest available purity. Enzymes for DNA restriction and modification are from New England Biolabs (Schwalbach, Germany), Boehringer (Mannheim, Germany), Stratagene (Heidelberg, Germany), or Pharmacia (Freiburg, Germany). Isolation and manipulation of DNA was performed as described (*11*). Oligonucleotides (including *tetO*) were obtained from PE Applied Biosystems (Weiterstadt, Germany). Sequencing was carried out according to the protocol provided by Perkin-Elmer for cycle sequencing and analyzed with an ABI PRISM 310 Genetic Analyzer (PE Applied Biosystems, Weiterstadt, Germany).

Bacterial Strains and Plasmids. All bacterial strains are derived from *E. coli* K12. Strain DH5α was used for general cloning procedures and strain RB791 for overexpression of TetR variants. The plasmid pWH1950(D) (*12*) is a pWH1950 (*13*) derivative carrying a *tetR*(D) gene under control of the *tac* promotor.

Construction of TetR Variants. TetR variants were constructed by directed PCR mutagenesis with the three-primer method according to (*14*). The conditions for the PCR reaction were adjusted as described (*15*). The obtained *tetR* genes were cloned into the TetR overexpression plasmid pWH1950(D) and sequenced to control the presence of desired mutations and the absence of other mutations.

Purification of TetR Variants. pWH1950(D) or pWH1950(D) derivatives were transformed into *E. coli* RB791. Cells were grown in 3 L of LB at 28 °C in shaking flasks. Tet repressors were overexpressed by adding isopropyl-1-thio-β-D-galactopyranoside to a final concentration of 1 mM at an OD_{600} of 0.7−1.0. Cells were pelleted, resuspended in buffer A (50 mM NaCl, 2 mM DTT, and 20 mM sodium phosphate buffer, pH 6.8), and broken by sonication, and TetR was purified by cation exchange chromatography using POROS HS/M Medium (PE Applied Biosystems, Weiterstadt, Germany) and gel filtration as described (*13*). The determination of protein concentrations was done by UV spectroscopy and saturating fluorescence titrations with atc.

Fluorescence Measurements. All fluorescence measurements were performed in a Spex Fluorolog with a double monochromator. To observe atc fluorescence, the excitation wavelength was set to 455 nm, and the emission was detected at 545 nm with a slit width of 4 mm. An internal rhodamine B standard (Kodak, Stuttgart) was used to correct intensity fluctuations of the Xenon Arc Lamp. Titrations with Mg^{2+} were done by adding Mg^{2+} stock solutions; atc titrations were carried out by adding different amounts of atc solutions to aliquots of a repressor dilution. All fluorescence measurements were carried out under equilibrium conditions at 28 °C in buffer K (100 mM Tris-HCl, pH 8.0, 100 mM NaCl, 0.1 or 1 mM EDTA). Free Mg^{2+} concentrations in EDTA-containing buffer were calculated as described (*16*).

UV Measurements for K_M Determination. UV titrations were carried out in buffer O (100 mM Tris-HCl, pH 8.0, 100 mM NaCl) at an atc concentration of 10 μM by adding $MgCl_2$ solutions into the cuvette. The absorption was detected in an Ultrospec 4000 (Pharmacia, Freiburg, Germany). A spectrum was recorded after each titration step. The data of the wavelength with the largest absorption change (334 nm) were taken to fit a rectangular hyperbolic binding function.

Calculation of Binding Constants K_T, K_{Mg}, and K_A. To perform the fits, the binding equilibria were applied as shown in the text. The binding constants were calculated with a least-squares fit method, minimizing

$$S^2 = \sum (F_{exp} - F_{theor})^2$$

where S^2 is the analysis of variance and F_{exp} and F_{theor} represent the experimental and theoretical fluorescence intensities, as described by (*17*). For the determination of K_{Mg} and K_A, the fits were performed for $\alpha = 1$ (no cooperativity in atc binding) and variable α. As no considerable cooperativity was detected ($\alpha \approx 1$), all data obtained with variable α were transformed according to the equation:

$$K_{\alpha=1} = \alpha^{0.5} \times K_{\alpha\ var}{}^2$$

For the calculation of K_T, no variation of α was applied.

40 bp Tet Operator Fragment. For generation of the 40 bp DNA fragment containing *tetO*, two oligonucleotides, 5′-GGGTGTGCCGAC**ACTCTATCATTGATAGAGT**-TATTATACC-3′ and 5′-CGGTATAATA**ACTCTATCAAT-GATAGAGT**GTCGGCACACC-3′ (the *tetO* nucleotides are written in boldface letters), were hybridized. Equal molar amounts of each oligonucleotide were mixed in a buffer containing 70 mM Tris, pH 7.6, 10 mM $MgCl_2$, and 5 mM DTT. The mixture was heated at 94 °C for 2 min and allowed to cool within 60 min to 4 °C.

Electrophoretic Mobility Shift Experiments. For the EMSA experiments, the synthetic 40 bp *tet* operator fragment was used. Complexation of Tet repressor variants and operator was performed for 20 min at ambient temperature. The concentrations were adjusted as follows: 0.5 μM *tetO*, 2.5 μM TetR monomer, 12.5 μM atc or tc, 1.25 mM $MgCl_2$ or EDTA, 2.5 mM NaCl, 1 mM DTT, 20 mM Tris, pH 8.0, 20 ng/μL nonspecific DNA. The mobility of the DNA was analyzed by electrophoresis on 8% polyacrylamide gels.

RESULTS

Binding of the $[Atc-Mg]^+$ Complex to TetR. To determine the binding constants, TetR(D) and atc were titrated with Mg^{2+} as has been described for tc and TetR(B) (*17*). We have used TetR(D) in this work to be able to discuss the results in light of the crystal structures obtained with this TetR variant, which is thought to have the same structure and functional properties as TetR(B) (*4*). To verify the underlying binding scheme, we have performed this titration at four different concentrations of TetR, and the results are shown in Figure 2. At the very low TetR concentration of 2.2 nM, which is the lowest possible concentration for this measurement because the fluorescence intensity is barely above the buffer background, we already see an increased fluorescence in the absence of Mg^{2+}, indicating atc−TetR interaction. This interaction seems to be increased at concentrations of 11 nM, 110 nM, and 1.1 μM TetR (see Figure 2). To account for this effect, we have modified the binding scheme of TetR, atc, and Mg^{2+} to include atc binding to TetR in the absence of Mg^{2+}.

Binding Scheme for the Analysis of Atc−Mg^{2+}−TetR(D) Interactions. Figure 3 shows the binding scheme of all possible interactions in a fluorescence titration of TetR with

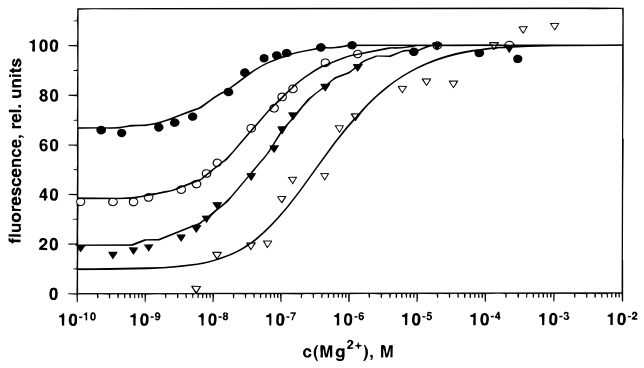

FIGURE 2: Fluorescence titrations of TetR and atc with Mg^{2+}. The symbols indicate TetR monomer concentrations of 1.1 μM (●), 0.11 μM (○), 11 nM (▼), and 2.2 nM (▽). The solid lines represent the corresponding fit. The fluorescence of the buffer was subtracted, and the fluorescence intensities were normalized.

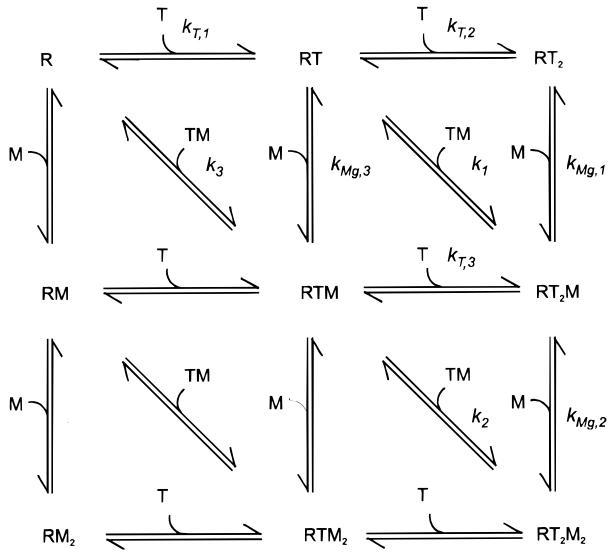

FIGURE 3: Binding scheme of all possible species containing TetR dimer (R), atc (T), and Mg^{2+} (M). The horizontal equilibria represent binding of atc; the diagonal and vertical equilibria binding of $[atc-Mg]^+$ and Mg^{2+}, respectively. Only the determined equilibrium association constants are shown in italics. The lower left part describes binding of Mg^{2+} to empty binding sites, which was not detected and consequently not considered in the calculations.

atc and Mg^{2+}. A free dimeric repressor (R) could first bind atc (T) or Mg^{2+} (M) or the $[atc-Mg]^+$ complex (TM) in one of its two binding pockets. As the ligand concentrations are increased, the different reaction pathways eventually lead to the complex (RT_2M_2). The ligand affinity of one binding pocket may depend on the occupation state of the other. This possibility was taken into account in several calculations described below; however, no hints for such cooperativity were detected.

The amounts of the different complexes existing at equilibrium at various concentrations of Mg^{2+} and atc are determined by the corresponding binding constants for the reactions in the pathways shown in Figure 3. Since no evidence for binding of Mg^{2+} to TetR has been obtained at the concentrations employed here, the lower left triangle of the binding scheme in Figure 3 can be neglected. The following equations cover all equilibria under this assumption:

$$TM = K_M \times T \times M \quad (1)$$

$$RT = K_{T,1} \times T \times R \quad (2)$$

$$RT_2 = K_{T,2} \times T \times RT \quad (3)$$

$$RTM = K_{A,1} \times TM \times R = K_{Mg,3} \times RT \quad (4)$$

$$RT_2M = K_{T,3} \times T \times RTM = K_{Mg,1} \times RT_2 \quad (5)$$

$$RT_2M_2 = K_{A,2} \times TM \times RTM = K_{Mg,2} \times RT_2M \quad (6)$$

and

$$T_{total} = T + TM + RTM + 2RT_2M_2 + RT + 2RT_2 + 2RT_2M \quad (7)$$

$$R_{total} = R + RTM + RT_2M_2 + RT + RT_2 + RT_2M \quad (8)$$

T_{total} and R_{total} are the respective total concentrations of atc and TetR. Theoretical binding curves were generated according to the equation:

$$F_{total} = F_0 + F_1 \times T + F_2 \times TM + F_3 \times (RTM + RT_2M + 2RT_2M_2) + F_4 \times (RT + RT_2M + 2RT_2) \quad (9)$$

in which F_{total} is the total fluorescence, F_0 is the buffer fluorescence, and F_1, F_2, F_3, and F_4 are the molar fluorescence intensities of free atc, $[atc-Mg]^+$, $[atc-Mg]^+$-complexed repressor, and atc-complexed repressor, respectively. The fluorescence properties of one TetR subunit are assumed to be independent of the other subunit. We have carried out titration experiments which allow the determination of K_M, K_T, K_{Mg}, and K_A.

Determination of K_M for Atc−Mg^{2+} Binding. Binding of Mg^{2+} to atc was assayed in titrations employing changes in UV absorption of atc, because its fluorescence lifetime changes upon binding of Mg^{2+}.[2] The binding constant K_M is $(3.35 \pm 0.13) \times 10^3$ M^{-1}. Thus, the concentration of free $[atc-Mg]^+$ is so low in all other titration experiments performed here that its contribution to the total fluorescence was neglected.

Determination of K_T for TetR−Atc Binding in the Absence of Mg^{2+}. The Mg^{2+}-independent atc equilibrium association constant with TetR(D) was determined by titration of 0.05 μM repressor dimer with atc in the presence of 20 mM EDTA. Atc fluorescence was employed to observe complex formation. The titration curve is shown in Figure 4A. Only eqs 2 and 3 are used to calculate theoretical binding curves, since no Mg^{2+} is present. Equations 7 and 8 can therefore be reduced to

$$T_{total} = T + RT + 2RT_2$$

and

$$R_{total} = R + RT + RT_2$$

The total fluorescence is then given by

$$F_{total} = F_0 + F_1 \times T + F_4 \times (RT + RT_2M + 2RT_2)$$

[2] M. Kunz, personal communication.

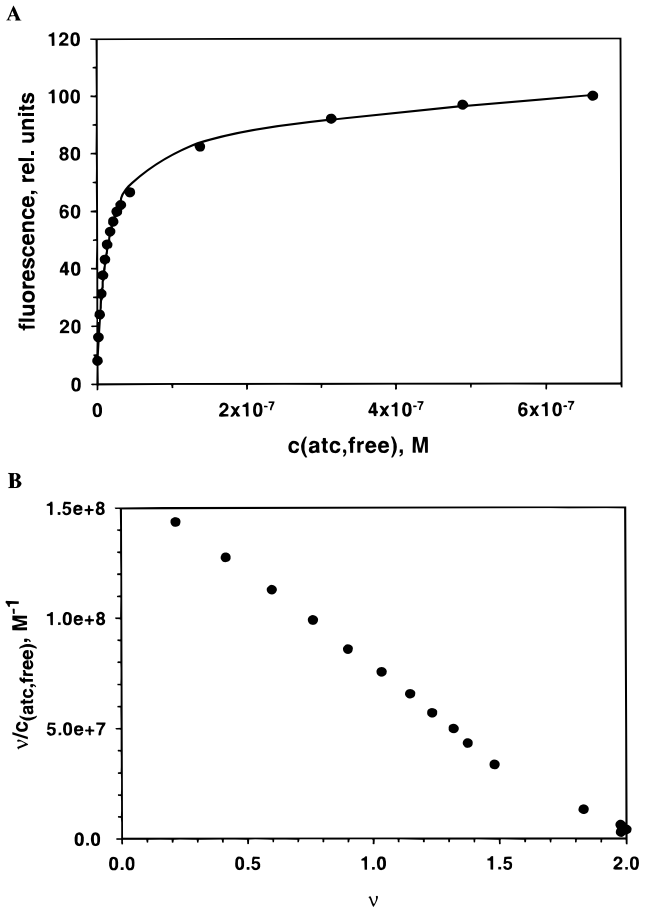

FIGURE 4: (A) Binding of TetR with atc determined by fluorescence titration at c(TetR) = 0.1 μM (monomer). The filled circles show the data; the line represents the fit for $K_T = 6.4 \times 10^7$ M^{-1}. To capture any contaminating Me^{2+} ions, the buffer contained 1 mM EDTA. (B) Scatchard plot of the same data. ν is the average number of atc molecules bound to one TetR dimer. The linearity of the graph shows the absence of cooperativity for the two atc binding sites.

K_T for atc and TetR binding is $(6.5 \pm 0.2) \times 10^7$ M^{-1}, which is more than 100-fold higher than for tc. The data nearly yielded a straight line in a Scatchard plot as shown in Figure 4B. Thus, no or almost no cooperativity is present, and the binding sites in TetR are probably thermodynamically identical.

Determination of K_{Mg} for Mg^{2+} Binding to the TetR−Atc Complex. To determine K_{Mg}, a 60-fold excess of atc (3 μM) over TetR dimer (0.05 μM) was used. Under these conditions, TetR is forced into the atc complex according to the equation:

$$RT_2 = K_{T,1} \times K_{T,2} \times T^2 \times R$$

Using a K_T of 6.5×10^7 M^{-1}, the equilibrium concentration of RT_2 is calculated as >0.0495 μM. Thus, the repressor is practically completely complexed with two atc molecules. Titration with Mg^{2+} was observed by the atc fluorescence. The resulting binding curve is shown in Figure 5. Two different methods of analysis were applied to the data to compare the results.

The very small amount of noncomplexed repressor was disregarded in the first analysis, assuming a bimolecular reaction. Fitting of a rectangular hyperbolic binding function yielded a K_{Mg} value of $(7.9 \pm 2.6) \times 10^7$ M^{-1}. Scatchard

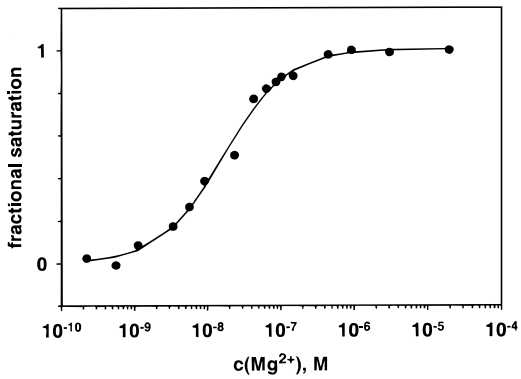

FIGURE 5: Fluorescence titration of the TetR−atc complex with $MgCl_2$ at c(TetR) = 0.1 μM (monomer) and c(atc) = 3 μM. The filled circles show the fractional saturation and the line the fit according to a rectangular binding function. The calculated binding constant K_{Mg} is 6×10^7 M^{-1}.

Table 1: Binding Constant for the Equilibrium R + 2TM ⇌ RT_2M_2[a]

c(atc), μM	c(TetR), μM	$K_A \times 10^{12}$ M^{-1}
1	1.1	1.2 ± 0.10
0.1	0.11	0.88 ± 0.16
0.01	0.011	1.0 ± 0.30
0.002	0.0022	0.72 ± 0.37

[a] The constants were determined by fluorescence titration with $MgCl_2$ at the listed atc and TetR concentrations.

analysis clearly showed the absence of cooperativity for the Mg^{2+} binding sites (not shown).

In the second method, K_{Mg} was calculated using the equilibria 1−9 from the complete binding scheme in Figure 3. To specifically consider Mg^{2+} binding to the TetR−atc complex, eqs 4−6, which include Mg^{2+}-containing complexes, have been modified to describe binding of free, not atc-bound, Mg^{2+}:

$$RTM = K_{Mg,3} \times M \times RT \quad (4a)$$

$$RT_2M = K_{Mg,1} \times M \times RT_2 \quad (5a)$$

$$RT_2M_2 = K_{Mg,2} \times M \times RT_2M \quad (6a)$$

Thus, only horizontal and vertical equilibria from the binding scheme in Figure 3 were employed. The K_{Mg} of $(7.8 \pm 1.8) \times 10^7$ M^{-1} obtained this way is identical to the result obtained from the simple fit of a bimolecular reaction.

Determination of K_A for Binding of $[Atc-Mg]^+$ to TetR. The analysis of the data shown in Figure 2 for calculating K_A can now be attempted using eqs 1−9 taking Mg^{2+}-independent atc binding to TetR into account. The following parts of eqs 4−6 are used:

$$RTM = K_1 \times TM \times R \quad (4b)$$

$$RT_2M = K_{T,3} \times T \times RTM \quad (5b)$$

$$RT_2M_2 = K_2 \times TM \times RTM \quad (6b)$$

The resulting K_A values determined at different TetR concentrations are presented in Table 1. Data from all four concentrations revealed identical results of 9.8×10^{11} M^{-1}

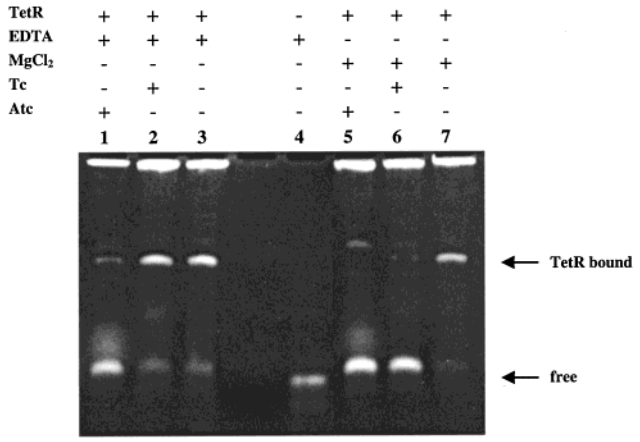

FIGURE 6: EMSA of *tet* operator with TetR. The *tet* operator fragment (lane 4) is complexed by TetR in the presence of EDTA or Mg^{2+} (lanes 3 and 7). Atc causes the release of *tetO* with or without Mg^{2+} (lanes1 and 5); tc induces only in the presence of Mg^{2+} (lanes 2 and 6). The band on top of the picture is caused by the nonspecific DNA. The diffuse signal appearing above free DNA in lanes 1 and 5 is due to atc fluorescence.

for $[atc-Mg]^+$ complex binding to TetR. This result demonstrates the validity of the binding scheme developed here.

This detailed study of the TetR−atc interaction reveals a different mode of inducer binding than was previously described for tc (*2*). The difference is in the remarkably high affinity of atc for TetR in the absence of Mg^{2+}. The ratio K_A/K_T of the binding constant with and without Mg^{2+} is about 10^4, the same as tc with $K_A \approx 10^9$ and $K_T \approx 10^5$. This indicates a similar contribution of Mg^{2+} to TetR binding for both compounds and leads to the question whether binding in the absence of a divalent cation is productive for induction or represents a nonproductive binding mode.

Electrophoretic Mobility Shift Analysis of the tetO−TetR Interaction Dependence of Atc and Mg^{2+}. The high Mg^{2+}-independent affinity of atc to TetR enables us to address the question whether induction of TetR is possible without a divalent cation. Atc binds TetR 500-fold better than tc. Therefore, the TetR−atc complex might be stable enough to observe release of the operator DNA in electrophoretic mobility shift analyses (EMSA) in the absence of Mg^{2+}. The results of the EMSA are displayed in Figure 6 and clearly demonstrate that *tetO* is not bound by TetR in the presence of atc, regardless of whether Mg^{2+} is present or not. The *tetO* fragment is almost quantitatively complexed by TetR with and without 5 mM Mg^{2+} in the absence of inducer (compare lane 4 with lanes 3 and 7 in Figure 6). Atc prevents complex formation; i.e., TetR is induced in the presence and absence of Mg^{2+} (lanes 1 and 5). The diffuse signal appearing above free DNA is due to atc fluorescence. When added in the same concentration as atc, tc prevents formation of the TetR−*tetO* complex only in the presence of Mg^{2+} (lanes 2 and 6). Thus, these results establish clearly that TetR can be induced by atc in the absence of Mg^{2+}. Therefore, the interactions of amino acid side chains in TetR with Mg^{2+} cannot be vitally important to trigger the conformational change necessary for induction.

Effects of Replacing Mg^{2+}- and Tc-Contacting Residues of TetR by Alanine on Inducer Binding. In the crystal structure of the TetR−$[tc-Mg]_2^+$ complex, the Mg^{2+} ion is engaged in a direct interaction with His100, and two of three water molecules coordinating Mg^{2+} form hydrogen bonds to the γ-oxygens of Glu147 (*7*). The third water molecule forms a hydrogen bond with the Oγ of Thr103. A Mg^{2+}-independent contact to tc is provided by Asn82, which forms hydrogen bonds to the A ring of tc. These interactions are depicted in Figure 1. We constructed four single alanine substitution mutants of TetR at these residues, TetR N82A, H100A, T103A, and E147A. The Mg^{2+}-dependent and -independent atc binding constants of these mutants were determined, and their in vitro inducibilities by tc and atc were analyzed by EMSA.

Table 2: Mg^{2+}-Independent and Mg^{2+}-Dependent Atc Binding Constants of Single Alanine Substitution Mutants

	$K_T \times 10^5\ M^{-1}$	$K_A \times 10^9\ M^{-1}$
TetR(D) wt	650 ± 14	980 ± 460
TetR(D) N82A	<1[a]	0.25 ± 0.02
TetR(D) H100A	260 ± 60	8.8 ± 0.65
TetR(D) T103A	14 ± 2	2.4 ± 0.21
TetR(D) E147A	220 ± 80	1.0 ± 0.1

[a] The Mg^{2+}-independent atc affinity of TetR N82A was too low to be quantified.

The binding constants of atc with these mutant proteins are presented in Table 2. Mg^{2+}-independent atc binding is only slightly (about 2-fold) reduced for TetR H100A and TetR E147A compared to wt TetR. TetR T103A shows an about 45-fold reduced affinity for atc, and that of TetR N82A is below the detection limit of $10^5\ M^{-1}$. Mg^{2+}-dependent binding is strongly reduced for all four mutants: TetR N82A exhibits a 4000-fold decreased binding constant, while TetR E147A shows 1000-fold and TetR T103A 400-fold reduced atc binding. The smallest reduction was determined for TetR H100A at 110-fold. Thus, the alanine substitutions at positions 100 and 147 selectively affect Mg^{2+}-dependent binding, whereas the exchange T103A shows a larger effect in Mg^{2+}-dependent binding than without the metal ion. N82A shows a general atc binding defect, and a possible Mg^{2+}-independent component cannot be detected because the respective constant is too small.

Effects of the Ala Substitutions on Induction. EMSA performed as described above with the four TetR mutants are shown in Figure 7. TetR T103A is not induced under these conditions, while TetR N82A shows some residual induction in the presence of atc and Mg^{2+}. TetR H100A and TetR E147A are inducible by atc with or without Mg^{2+}, while tc does not induce any of these mutants, not even when Mg^{2+} is present. This result shows that induction by atc without Mg^{2+} parallels the respective affinities (see Table 2). This is not the case for Mg^{2+}-dependent binding: Although TetR T103A has a higher affinity for $[atc-Mg]^+$ than TetR E147A, no induction was detected.

DISCUSSION

Atc is a precursor of tc biosynthesis and is derived from it by the dehydration of the C-ring with the elimination of H_2O between C6 OH and the 11A H, rendering the C-ring aromatic (Figure 1). Despite these rather small changes, atc binds TetR with a 500-fold higher affinity than tc, both in the presence and in the absence of Mg^{2+}. Favorable interactions of atc compared to tc with TetR may result from the lack of the hydroxyl grouping at position 6, which in the

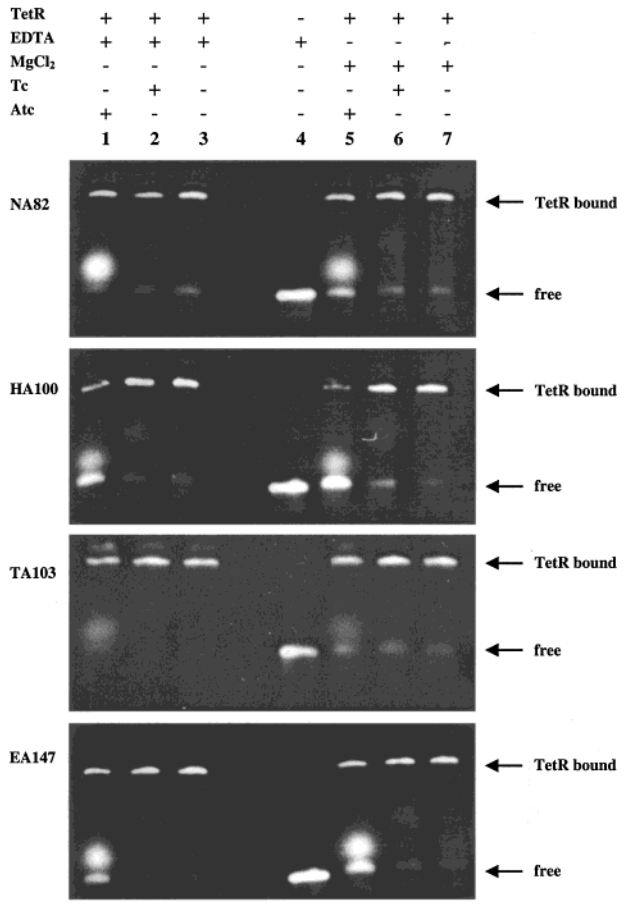

FIGURE 7: EMSA for TetR N82A, TetR H100A, TetR T103A, and TetR E147A. All four TetR variants show *tetO* binding. TetR N82A and T103A are not inducible; H100A and E147A are only inducible with atc.

crystal structure points toward the side chain of Val113, making an energetically unfavorable contact. Furthermore, the methyl grouping at position 6 is planar with respect to the C-ring in atc, making a favorable interaction with the Val113 side chain (*5*). Thus, the increased affinity has a structural resemblance.

Mg^{2+}-limited titration experiments at micromolar concentrations are more complex than previously described for tc (*2*), because Mg^{2+}-independent binding of atc to TetR must be considered. The K_T of $(6.5 \pm 0.2) \times 10^7$ M^{-1} shows that in the absence of Mg^{2+} 70% of the repressor is complexed with two atc molecules at micromolar concentrations. Two assumptions were made to interpret the fluorescence measurements using the proposed binding model: (i) The fluorescence increase from binding any species (i.e., atc, Mg^{2+}, $[tc-Mg]^+$) to one subunit of the TetR dimer is independent of the occupation state of the other subunit; (ii) the microscopic constants k_3, $k_{T,3}$, and $k_{Mg,3}$ (see Figure 3) not directly accessible by fluorescence experiments are equal to k_1, $k_{T,1}$ and $k_{Mg,1}$. The first assumption cannot be proven because a mixture of repressor molecules in different binding states is always present at equilibrium. Since the affinity of the second atc might be altered by the occupation state of the other binding pocket, this effect was considered in the model by including the cooperativity factor α for the TetR$-$$[atc-Mg]^+$ and $[TetR-atc]-Mg^{2+}$ reactions, allowing k_2 and $k_{Mg,2}$ to differ from k_1, and $k_{Mg,1}$, respectively. The absence of cooperativity for Mg^{2+}-independent atc binding ($k_{T,1} = k_{T,2}$) is demonstrated via the straight line in the Scatchard plot (see Figure 4B). Since the best fits result in α (see M+M) values near unity in both cases, no cooperativity is needed to interpret the data. Thus, assumption (ii) is justified.

Scheme 1

'diagonal way'		'orthogonal way'	
$T + M = TM$	$K_M = 3.4 \times 10^3$	$R + T = RT$	$K_T = 6.5 \times 10^7$
$R + TM = RTM$	$K_A = 9.8 \times 10^{11}$	$RT + M = RTM$	$K_{Mg} = 8.6 \times 10^7$
$R + T + M = RTM$	$K_{total} = 3.3 \times 10^{15}$	$R + T + M = RTM$	$K_{total} = 5.6 \times 10^{15}$

Two reaction pathways lead from free repressor to the ternary complex: Either atc and Mg^{2+} bind subsequently to TetR (horizontal and vertical equilibria in the binding scheme in Figure 3), or the $[atc-Mg]^+$ complex binds to TetR (diagonal route). The binding constants for both reaction pathways are compared in Scheme 1. Both pathways lead to the same result for K_{total}, suggesting that $[atc-Mg]^+$ is bound with the very high constant of $\sim 1 \times 10^{12}$ M^{-1}. This makes atc the highest affinity inducer for TetR of all tc derivatives tested so far. The excellent fit of the data and the consistency of the obtained binding constants suggest that the reaction scheme outlined in Figure 3 is sufficient to completely describe atc binding to TetR.

The four Ala substitution mutants were designed to check Mg^{2+}-specific effects in TetR H100A, T103A, and E147A, while N82A contacts tc directly and should serve as a control expected to show the same effects on induction with and without Mg^{2+} (*5*, *7*). The latter assumption is verified by the general inductive defect of TetR N82A, but only two out of the Mg^{2+}-contacting mutations, TetR H100A and E147A, behave as expected. They show a decrease of Mg^{2+}-dependent atc binding (*5*, *7*). This is roughly 4-fold larger for TetR E147A than for TetR H100A (Table 2), in agreement with the loss of two Mg^{2+} coordinations for TetR E147A and one for TetR H100A. TetR T103A does not show the expected properties. Compared to TetR E147A, this mutant has a lower Mg^{2+}-independent, but a higher Mg^{2+}-dependent atc binding constant. Thus, the Thr103 residue is involved in tc binding via Mg^{2+} complexation (*7*) and must undergo an alternative interaction with atc in the absence of Mg^{2+}.

Furthermore, the induction seen with TetR H100A and TetR E147A in the absence of Mg^{2+} leads to the conclusion that the interactions of Mg^{2+} with amino acids His100 and Glu147, and also Mg^{2+} itself, are not vital to trigger the conformational change necessary for induction. This is also different for TetR T103A, which is not induced, although the Mg^{2+}-dependent atc affinity should be high enough to saturate the protein, as shown by the induction of TetR E147A having a similar affinity for atc. His100 and Thr103 are thought to be the first residues that change position upon tc binding (*6*, *7*). We conclude, in good agreement with the structural data, that the Thr103 residue has a trigger function for induction. On the other hand, Mg^{2+} does not have such a function. Furthermore, this trigger function is also not seen for His100. This residue just increases the affinity of TetR for $[atc-Mg]^+$. In addition to information hitherto available from the crystal structures, the reduced Mg^{2+}-independent atc affinity for TetR N82A and TetR T103A indicates that Thr103, like Asn82, interacts with atc also in the absence of Mg^{2+}. The presence of Mg^{2+} leads to an 10 000-fold

increased affinity of TetR for tc or atc. Since atc has a larger Mg^{2+}-independent affinity for TetR, induction occurs in a concentration range accessible for EMSA analysis. Thus, these new mechanistic insights could not be seen with tc.

The results presented here indicate that the Mg^{2+}-dependent mechanism of TetR induction as revealed by the X-ray structures (*7*) may be not the only one. We propose an alternative induction pathway in the absence of divalent metal ions. Like the known pathway, this also requires the Thr103 residue, but not His100 or Glu147. We attempt to crystallize a TetR−atc complex in the absence of divalent metal ions to shed light on this alternative induction mechanism.

ACKNOWLEDGMENT

We thank Dr. M. Takahashi for many fruitful discussions, Marco Reich for technical assistance, and Kirsten Oliva for proofreading the manuscript.

REFERENCES

1. Schnappinger, D., and Hillen, W. (1996) *Arch. Microbiol. 165*, 359−369.
2. Takahashi, M., Altschmied, L., and Hillen, W. (1986) *J. Mol. Biol. 187*, 341−348.
3. Ettner, N., Metzger, J. W., Lederer, T., Hulmes, J. D., Kisker, C., Hinrichs, W., Ellestad, G. A., and Hillen, W. (1995) *Biochemistry 34*, 22−31.
4. Hinrichs, W., Kisker, C., Duvel, M., Muller, A., Tovar, K., Hillen, W., and Saenger, W. (1994) *Science 264*, 418−420.
5. Kisker, C., Hinrichs, W., Tovar, K., Hillen, W., and Saenger, W. (1995) *J. Mol. Biol. 247*, 260−280.
6. Orth, P., Schnappinger, D., Hillen, W., Saenger, W., and Hinrichs, W. (2000) *Nat. Struct. Biol. 7*, 215−219.
7. Orth, P., Saenger, W., and Hinrichs, W. (1999) *Biochemistry 38*, 191−198.
8. Orth, P., Cordes, F., Schnappinger, D., Hillen, W., Saenger, W., and Hinrichs, W. (1998) *J. Mol. Biol. 279*, 439−447.
9. Oliva, B., Gordon, G., McNicholas, P., Ellestad, G., and Chopra, I. (1992) *Antimicrob. Agents Chemother. 36*, 913−919.
10. Gossen, M., and Bujard, H. (1993) *Nucleic Acids Res. 21*, 4411−4412.
11. Sambrook, J., Fritsch, E. F., and Maniatis, T. (1989) *Molecular Cloning*, Cold Spring Harbor Laboratory Press, Cold Spring Harbor, NY.
12. Tiebel, B., Aung-Hilbrich, L. M., Schnappinger, D., and Hillen, W. (1998) *EMBO J. 17*, 5112−5119.
13. Ettner, N., Muller, G., Berens, C., Backes, H., Schnappinger, D., Schreppel, T., Pfleiderer, K., and Hillen, W. (1996) *J. Chromatogr. A 742*, 95−105.
14. Landt, O., Grunert, H. P., and Hahn, U. (1990) *Gene 96*, 125−128.
15. Berens, C., Schnappinger, D., and Hillen, W. (1997) *J. Biol. Chem. 272*, 6936−6942.
16. Perrin, D. D., and Dempsey, B. (1974) *Buffers for pH and Metal Ion Control*, Chapman and Hall, London.
17. Takahashi, M., Degenkolb, J., and Hillen, W. (1991) *Anal. Biochem. 199*, 197−202.

BI001018P